Materials Science and Engineering A 549 (2012) 20–29

Contents lists available at SciVerse ScienceDirect

Materials Science and Engineering A

journal homepage: www.elsevier.com/locate/msea

Influences of deformation strain, strain rate and cooling rate on the Burgers orientation relationship and variants morphology during β → α phase transformation in a near α titanium alloy

D. He[a], J.C. Zhu[a,*], S. Zaefferer[b], D. Raabe[b], Y. Liu[a], Z.L. Lai[a], X.W. Yang[a]

[a] National Key Laboratory for Precision Hot Processing of Metals, Harbin Institute of Technology, Harbin 150001, PR China
[b] Max-Planck-Institut für Eisenforschung, Abteilung Mikrostrukturphysik und Umformtechnik, Max-Planck-Strasse 1, 40237 Düsseldorf, Germany

ARTICLE INFO

Article history:
Received 25 November 2011
Received in revised form 2 March 2012
Accepted 20 March 2012
Available online 11 April 2012

Keywords:
Deformation strain
Strain rate
Cooling rate
Burgers orientation relationship
Variants morphology

ABSTRACT

High temperature compression deformation studies of Ti–6Al–2Zr–1Mo–1V titanium alloy in full β phase region with different strains/strain rates and then with subsequent varied cooling rates were performed to understand the microstructure evolution. Crystal orientation information and microstructure morphology of all tested samples were investigated by electron backscatter diffraction (EBSD) measurements. The crystal orientations of prior high temperature β grains were estimated by reconstructing the retained β phase at room temperature. The theoretical crystal orientations of all possible α variants within an investigated prior β grain were calculated according to the Burgers orientation relationship (OR) between parent and product phase. The calculated and experimental results were then compared and analyzed. The influences of deformation strain, strain rate and cooling rate on the Burgers OR between prior β matrix and precipitated α phase were investigated. Full discussions have been conducted by combination of crystal plasticity finite element method (CP-FEM) grain-scale simulation results. The results indicate that external factors (such as deformation strain, strain rate and cooling rate) have a slight influence on the obeying of Burgers OR rule during β → α phase transformation. However, strain rate and cooling rate have a significant effect on the morphology of precipitated α phase.

1. Introduction

Titanium and titanium alloys are preferentially used in the aerospace sector, chemical industry, medical engineering, and leisure sector because of their high specific strength and excellent corrosion resistance [1]. Titanium alloys are classified as α, near α, α + β, and β alloys according to their position in a pseudo-binary section through a β-isomorphous phase diagram [2]. TA15, whose nominal chemical component is Ti–6Al–2Zr–1Mo–1V, is one of the typical near alpha titanium alloys and is widely used in aerospace industry owing to its excellent thermal stability and low fatigue crack growth rate [3].

The general production process of titanium alloys includes melting, casting, forging, and subsequent heat treatments. However, due to high yield stress and relatively low elastic modulus, most of titanium alloys (including TA15) are difficult to deform at room temperature. Therefore, their fabrication and forming operation are usually carried out at elevated temperatures, such as α + β forming (at temperature of 30–100 °C below the β-transus), β deforming (at temperature above the β-transus). For TA15 titanium alloy, whose microstructures cannot be significantly manipulated by traditional heat treatment, thermomechanical processing was usually adopted to get the desired usable shape and control the microstructure [4]. Moreover, local transformation from prior body-centered cubic (bcc) β phase to hexagonal close-packed (hcp) α phase of TA15 titanium alloy is generally governed by the Burgers orientation relationship [5]: $\{1\,1\,0\}_\beta//\{0\,0\,0\,1\}_\alpha$, $\langle 1\,1\,1\rangle_\beta//\langle 1\,1\,\bar{2}\,0\rangle_\alpha$. The special Burgers OR also has a significant effect on texture inheritance and crystallographic variant selection during the β → α phase transformation [6–9].

As reported in many research works [1,2,10], the microstructures have a substantial influence on the in-service and mechanical properties of titanium alloys. Generally, the lamellar microstructures exhibit excellent fracture toughness and high fatigue crack propagation resistance but low resistance to fatigue crack nucleation and poor plasticity. Even for lamellar microstructure, its mechanical properties are dramatically sensitive to microstructural parameters such as the size of α colonies, the ratio of width and length and the crystallographic orientation distribution [11].

* Corresponding author. Tel.: +86 451 86413792; fax: +86 451 86413922.
E-mail address: fgms@hit.edu.cn (J.C. Zhu).

0921-5093/$ – see front matter © 2012 Elsevier B.V. All rights reserved.
http://dx.doi.org/10.1016/j.msea.2012.03.110

In view of the above, influence of the processing parameters on the evolution of subsequent microstructure morphology, texture inheritance, and variant selection in these alloys, becomes a main research focus. The influences of deformation rate on the microstructure morphology were investigated by Seshacharyulu and Dutta [12]. Their research results reveal that the prior deformation rate has a significant influence on the morphology of transformed α: lamellar α grains formed at low strain rate (less than 10^{-1} s^{-1}) and coarse equiaxed α grains formed at high strain rate (1–100 s^{-1}) [12]. The influences of strain and strain rate on the β → α phase transformation kinetics, including the nucleation sites, nucleation numbers and growth rates of the α precipitations during subsequent cooling, were fully studied by a calculation model developed by Da Costa Teixeira et al. [13]. It is reported that, when an external field exists, such as a prior strain field induced by compression ($\varepsilon = -1.4$) in α + β phase field of TIMETAL 834 alloy, the Burgers OR between the primary α (α_p) and the retained β phase (β_r) was respected only up to 30–60% with a tolerance of 10° [14]. Some studies also indicate that elastic anisotropy could be decisive factor for the variant selection and has a relationship with the sharp textured regions called macrozones [15]. At the same time, Kato et al. [16] has observed that the stress always plays an important role in the early stage of α to β phase transformation process. On the other hand, some authors pointed out that the significant variant selections can occur during bcc to hcp phase transformation even if no external field is imposed [17].

Most of the early research work was focused on the morphology, growth direction and orientation selection of α lamellae or colonies during the deformation or heat treatment process. However, a clear understanding of the influence of the external factors on the respecting of Burgers OR between α and β phases during phase transformation is still not available. In the present work, the compression deformation tests with different strains/strain rates and different subsequent cooling rates were carried out on TA15 titanium alloy at 1050 °C. Based on the results obtained with different test parameters, the influences of deformation strain, strain rate, cooling rate on the obeying of Burges OR were analyzed. Finally, full discussions were conducted by combination of CP-FEM simulation results at grain-scale.

2. Experimental

2.1. Material and sample preparation

TA15 titanium bar stock having a chemical composition of 6.47 wt% Al, 1.59 wt% Zr, 1.45 wt% Mo, 1.91 wt% V, 0.038 wt% Fe and titanium balance was used in the present study. The β-transus temperature was around 993 °C. The as-received material was subjected to β forging at 1050 °C and was subsequently annealed at 600 °C for 4 h. The microstructure of the used alloy consisted of coarse primary α phase and residual β phase (less than 10 vol.%).

Cylindrical specimens of 5 mm diameter and 10 mm height for hot compression tests were machined from the mentioned bar stock.

2.2. Compression test

Uniaxial compression tests were carried out on a computer controlled servo-hydraulic testing machine (INSTRON 8501) equipped with induction heating apparatus and cooling systems. The compressive strain, strain rate and heating/cooling rate were exactly controlled by the testing machine during the test. All tests were conducted under the vacuum conditions. The test details are listed in Table 1. All test were performed at 1050 °C (~60 °C above β transus) which was achieved with 10 °C/s heating rate and deformation was started after 2 min holding at this temperature.

Table 1
The test no. and detailed test parameters in the present work.

Test no.	Strain	Strain rate (s^{-1})	Cooling rate (°C/s)
A	–	–	5
B	0.8	1	5
C	0.1	1	50
D	0.8	10	1

2.3. EBSD measurement

The deformed specimens were sectioned along compression axis into two equal halves. The sectioned surface was then prepared for scanning electron microscopy (SEM) and electron backscatter diffraction (EBSD) measurement using standard grinding and polishing techniques. A mixture of colloidal silica (OP-S, 90 vol.%) and H_2O_2 (10 vol.%) was used as a polishing solution during the final polishing process.

EBSD data acquisition was carried out on a JEOL 6500F scanning electron microscope equipped with an EBSD system developed by EDAX/TSL®. The Kikuchi patterns were indexed automatically in real time and the results were analyzed by the same software EDAX-TSL OIM®. In order to facilitate comparison, the central area of each prepared surface was selected to carry out EBSD measurement.

3. Results

3.1. Influence of deformation strain

The result of orientation image microscopy (OIM) with a scanning step size of 0.2 μm of sample A, which has not be subjected to any deformation, is shown in Fig. 1(a). The microstructure very clearly shows the presence of α lamellae along with a small fraction of residual β phase. These lamellae are 3–5 μm thick and 50–70 μm long in size. Some of lamellae even cross the whole prior β grain. The α colonies, which are composed of several parallel α lamellae sharing similar crystal orientation, nucleate preferentially at β grain boundaries and grow into the β grain interior until they impinge with other colonies, as seen in Fig. 1(a). The occurrence of similar microstructure was also observed in the previous studies [6,8,9,12,13,18].

We can easily deduce that there is an equiaxed prior β grain (marked as "Grain A", see Fig. 1(a) and (b)) in the center of the measured region from the distribution of grain boundary α lamellae. The sketch of the reconstructed β grain boundaries at high temperature has been plotted according to the residual β phase orientations and grain boundary α lamellae, as shown in Fig. 1(b). The reconstructed microstructure indicates that the microstructure at 1050 °C consists of equiaxial β grains of roughly 100–120 μm in size.

As mentioned in the introduction, the Burgers OR should be generally maintained during the transformation between the β phase and α phase. Owing to the cubic symmetry, 24 hexagonal variants of α should be obtained. Actually, taking both the cubic and hexagonal symmetries into consideration, there are only 12 distinct variants [5]. But here, our study revealed the presence of only 7 distinct variants in the marked "Grain A". Two possible reasons can account for the observed results. Firstly, the preferred selection of variant exists during the formation process of α lamellae even there in the absence of external influence [17]. Secondly, Fig. 1 gives only a 2 dimensional (2D) section; therefore, some information on other variants in real 3 dimensional (3D) spaces may be lost. However, our research objective is to study whether the Burgers OR is well

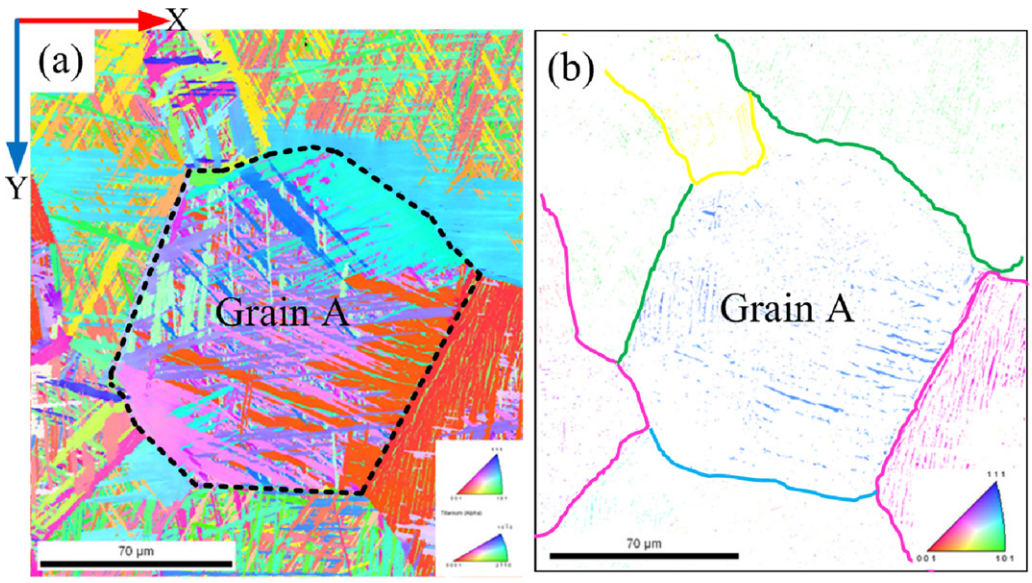

Fig. 1. Orientation map of sample A with 2 min holding at 1050 °C, without compression deformation, 5 °C/s cooling rate. Map color code: *Y* direction. (a) Inverse pole figure colored (IPF) orientation map of α and β phase. The area surrounded with a black dashed line shows a prior β marked "Grain A". (b) Residual β phase and the sketch of reconstructed β grain boundary at 1050 °C. (For interpretation of the references to color in the figure caption and text, the reader is referred to the web version of the article.)

respected under different external factors. So, how many of them (12 distinct α variants) appeared in the measured zone does not influence our results and analysis.

Fig. 2(a) gives {0 0 0 1} pole figure showing the crystal orientations of residual β in "Grain A". The crystal orientations of all possible α variants in "Grain A" were calculated according to Burgers OR rule with reference to the residual β phase orientation. The calculation results were plotted in {0 0 0 2} and {1 1 $\bar{2}$ 0} pole figures as red circles, as seen in Fig. 2(b).

Because a relatively small step size was used in the current EBSD measurement, a lot of orientation data was obtained for every group of α variant. To facilitate comparison with the calculated results, one hundred groups of crystal orientation data for each variant were randomly selected to represent the experimental orientation results. The processed experimental results were plotted as dots with different colors in the same {0 0 0 2} and {1 1 $\bar{2}$ 0} pole figures.

Fig. 2(b) shows that orientation distribution of the dots for each variant is relatively close. All dots (experimental results) fall into the red circles (theoretical calculation results). We can essentially make two important observations from Fig. 2(b). Firstly, the crystal orientation of every variant group is relatively identical. Secondly, the Burgers OR is perfectly obeyed during the β → α phase transformation, when there is no influence of prior deformation and the cooling rate is relatively slow (5 °C/s).

To investigate the influence of prior β deformation strain on Burgers OR during β → α phase transformation, uniaxial compression test were conducted on sample B at 1050 °C up to strain of 0.8 at a strain rate of 1 s^{-1}. The cooling rate is the same as that for sample A (5 °C/s), as shown in Table 1.

The orientation and image quality (IQ) map of sample B are shown in Fig. 3(a) and (b), respectively. There is no substantial difference in microstructure morphology between sample B and A. The microstructure of sample B was also composed of thin (2–4 μm) but long (~60 μm in max.) α lamellae and a small fraction of residual β layers. These results indicate that, for TA15 titanium alloy, the prior β deformation strain has no significant influence on the morphology of α variant, under conditions of low strain rate and slow cooling rate.

Ten distinct variants were detected in the marked "Grain B", as shown in Fig. 3(a). Before calculating the possible variants'

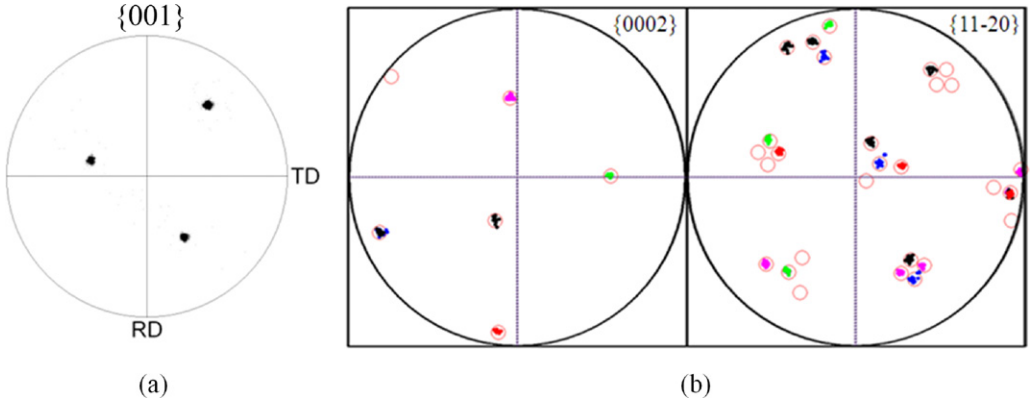

Fig. 2. (a) The {0 0 0 1} pole figure of residual β phase in marked "Grain A". (b) The {0 0 0 2} and {1 1 $\bar{2}$ 0} pole figures of seven α variants in marked "Grain A". The red circles and different color dots represent the theoretical calculation crystal orientation results for all possible α variants and experimental results, respectively. (For interpretation of the references to color in the figure caption and text, the reader is referred to the web version of the article.)

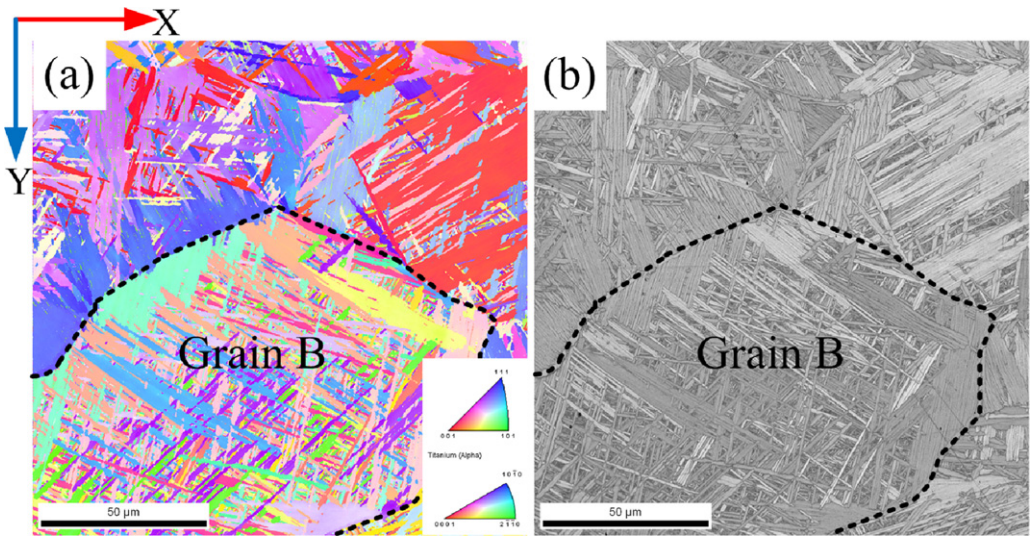

Fig. 3. (a) Orientation map of central zone in sample B, with 0.8 compression deformation strain at 1050 °C, 1 s^{-1} strain rate, 5 °C/s cooling rate after deformation, map color code: *Y* direction. The area surrounded with a black dashed line shows a prior β marked "Grain B". (b) Corresponding IQ map of central area in sample B. (For interpretation of the references to color in the figure caption and text, the reader is referred to the web version of the article.)

orientation, we must make sure whether the sub-grain was formed or not in the prior "Grain B" during compression deformation at 1050 °C. Since we could not get the crystal orientation information of "Grain B" upon post-deformation at 1050 °C, the residual β phase at room temperature was used to evaluate the high temperature situation. The crystal orientations of all residual β phase in "Grain B" were expressed in {0 0 1} pole figure, as seen in Fig. 4(a). Obviously, the residual β phase in "Grain B" are mainly orientated around (6 9 1)[$\bar{3}$ 1 9] crystal orientation. This means that no obvious sub-grain was formed in "Grain B" at 1050 °C for a prior compression strain of 0.8. Therefore the influence of sub-grain can be neglected when we calculate the crystal orientations of possible α variants. The mean value of all residual β phase orientations in "Grain B" was used to calculate the orientations of all possible α variants.

Results from both the theoretical calculation and measurements were plotted in the same {0 0 0 2} and {1 1 $\bar{2}$ 0} pole figure, as shown in Fig. 4(b). Again, all of the different color dots perfectly fall into to the red circles region. These results indicate that the Burgers OR is exactly obeyed during the β → α phase transformation, even though the prior β grain underwent relatively severe plastic deformation (sample B with 0.8 compression strain).

3.2. Influence of cooling rate

In order to evaluate the cooling rate influence, test C was designed and conducted. The details of experimental parameters are listed in Table 1. Compared with tests A and B, the obvious difference of test C is the high cooling rate (50 °C/s). One may doubt about the comparability of the results between the test C and B/A for investigating the influence of cooling rate. However, according to our previous analysis, the deformation strain has no significant influence on the morphology and Burgers OR obeying of α variant; therefore the results of test C are suitable and comparable.

The orientation and IQ map of sample C are presented in Fig. 5(a) and (b), respectively. Obviously, α lamellae are thinner and shorter when compared with those of sample A and B. There are rarely α laths crossing the whole prior β grain. This indicates that the cooling rate has an obvious effect on the size and morphology of α lamellae.

The crystal orientations of residual β phase in "Grain C" seem to be a little scattered, as can be seen from the region marked with a red ellipse in Fig. 6(a). According to the data analysis, the crystal orientations of residual β phase in marked "Grain C" can be divided into two groups. The average value of each group was calculated

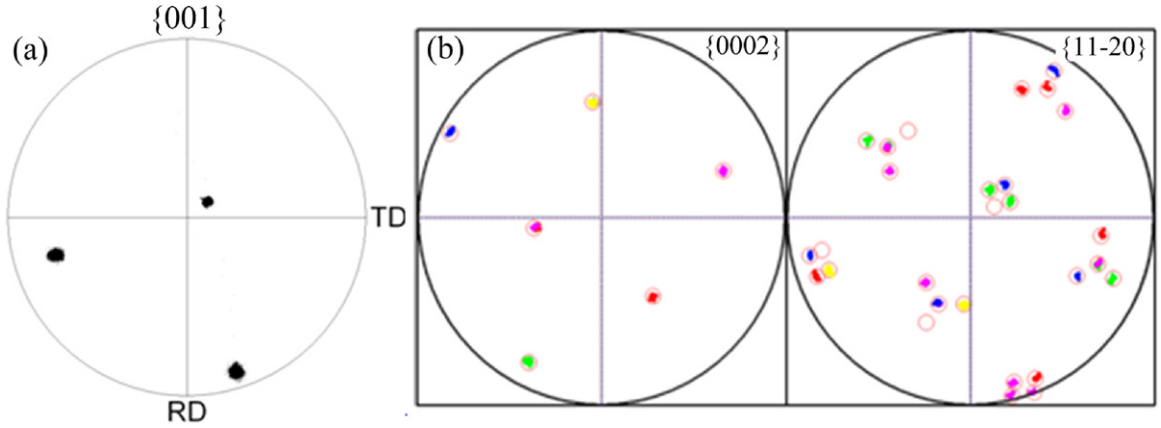

Fig. 4. (a) The {0 0 1} pole figure of residual β phase in marked "Gain B". The orientations are concentrated around (6 9 1)[$\bar{3}$ 1 9] crystal orientation. (b) The {0 0 0 2} and {1 1 $\bar{2}$ 0} pole figures of α variants appeared in marked "Grain B". The red circles and different color dots represent the theoretical calculation and experimental results, respectively. (For interpretation of the references to color in the figure caption, the reader is referred to the web version of the article.)

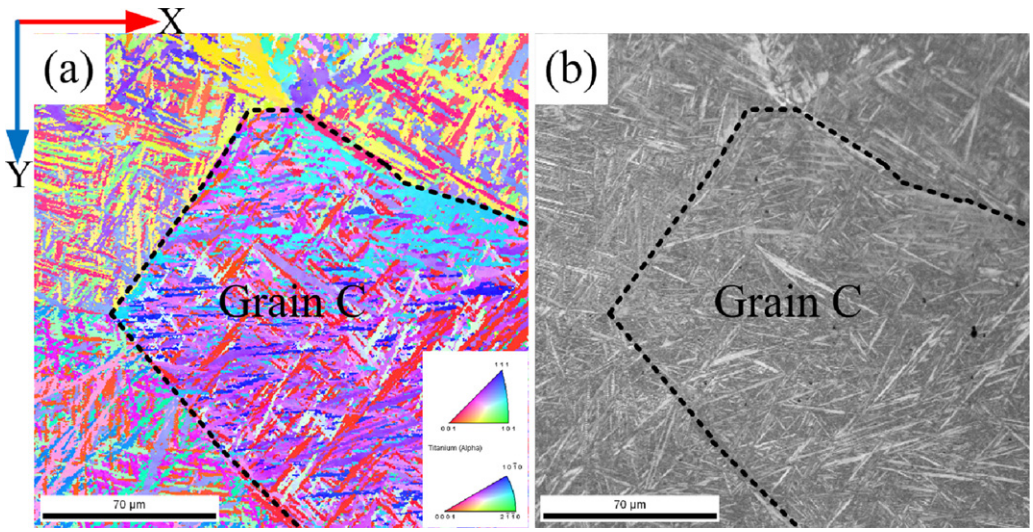

Fig. 5. (a) Orientation map of sample C, with a compression deformation strain of 0.1 at 1050 °C, 1 s^{-1} strain rate, 50 °C/s cooling rate after deformation, map color code: *Y* direction. The area surrounded with a black dashed line shows a prior β marked "Grain C". (b) Corresponding IQ map of central area in sample C. (For interpretation of the references to color in the figure caption and text, the reader is referred to the web version of the article.)

respectively and was used to evaluate the crystal orientations of all possible α variants. The calculated results of two groups were obtained and plotted in {0 0 0 2} and {1 1 $\bar{2}$ 0} pole figure by red and blue circles, respectively, as shown in Fig. 6(b).

It is seen that the experimental results (different color dots) are slightly scattered and some of them are even shifted out of red or blue circles. However, almost all of the dots still fall into the red or distribute near the blue circles. Taking experiment error into consideration, the Burgers OR is still generally respected during α precipitated from β phase process in the cause of high cooling rate (50 °C/s). This means that the cooling rate also does not have a significant influence on the obeying of Burgers OR rule during the β → α transformation of titanium alloys.

3.3. *Influence of strain rate*

To investigate the strain rate influence on microstructure morphology and Burgers OR obeying situation, the compression deformation at 1050 °C was conducted on sample D up to strain of 0.8 at a strain rate of 10 s^{-1}. The test parameters are listed in Table 1, line 4.

The OIM and IQ map are presented in Fig. 7(a) and (b), respectively. The microstructures are composed of grain boundary α lamellae, interior grain α variants and residual β layers. It should be noted that, these α lamellae are 30–50 μm in length and no lamellae crossing the whole prior β can be observed in marked "Grain D" (see Fig. 7). Compared with results of test A and B, the lamellae lengths of sample D are distinctly shorter, although prior β grains from which α lamellae precipitated are relatively close in size for all cases, as shown marked "Grain A", "Grain B" and "Grain D" in Figs. 1, 3 and 7, respectively. Thus, the deformation strain rate can influence the morphology of α lamellae, i.e., the length decreases with increasing strain rate. These results agree well with the Seshacharyulu's study: the morphology of α grain was changed from lamella to equiaxed grain when the stain rate increased from low value ($\leq 10^{-1}$ s^{-1}) to high (1–100 s^{-1}) [12]. One may ask whether it is induced by slow cooling rate. However, according to our discussion in the last section, the slow cooling rate will promote the growth of α lamellae.

The crystal orientation of residual β phase in marked "Grain D" is presented in {0 0 1} pole figure in Fig. 8(a). Five types of distinct α variants appeared in marked "Grain D". Both measured (different color dots) and calculated (red circles) results of crystal orientations of α variants in "Grain D" are displayed in {0 0 0 2} and {1 1 $\bar{2}$ 0} pole figures, as seen in Fig. 8(b). All of the experimental dots fall into the red circle regions. Obviously, although the compression deformation rate is much higher than that in the cases of samples

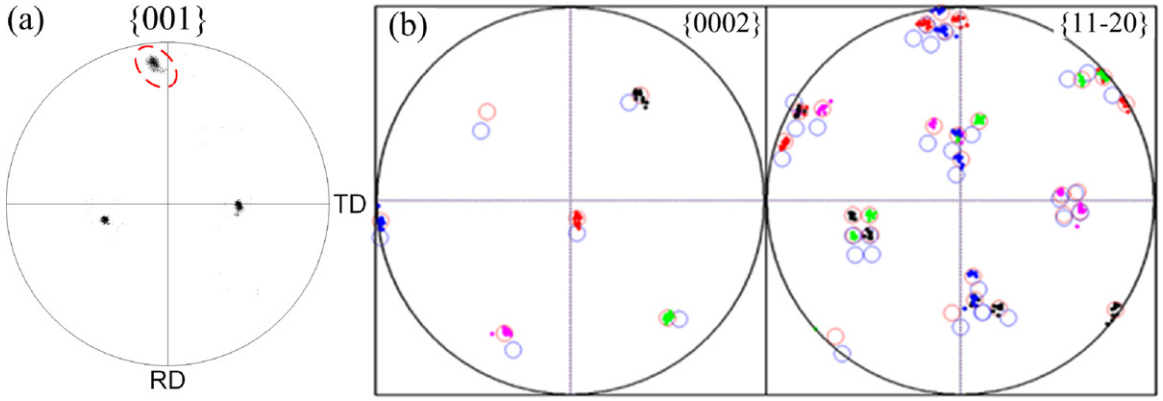

Fig. 6. (a) The {0 0 1} pole figure of residual β phase in marked "Gain C". The dots seem a little scattered, as seen the red line ellipse indicated position. (b) {0 0 0 2} and {1 1 $\bar{2}$ 0} pole figures of α lamellae. The red/blue circles and different dots represent the theoretical calculation and experimental results, respectively. (For interpretation of the references to color in the figure caption and text, the reader is referred to the web version of the article.)

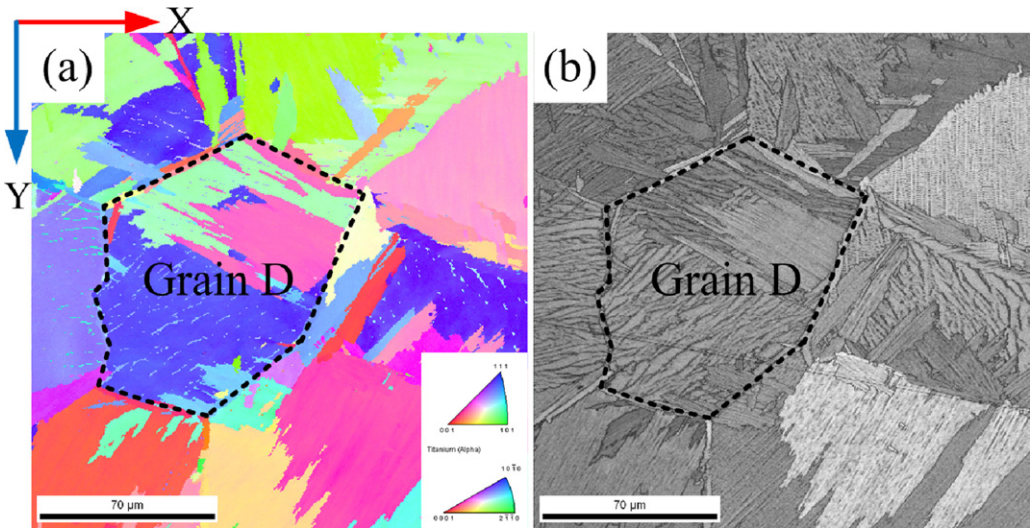

Fig. 7. (a) OIM map of sample D, 2 min holding at 1050 °C, with 0.8 compression deformation strain and 10 s^{-1} strain rate, 1 °C/s cooling rate after deformation, map color code: *Y* direction. The area surrounded with a black dashed line shows a prior β marked "Grain D". (b) The corresponding IQ map of sample D. (For interpretation of the references to color in the figure caption and text, the reader is referred to the web version of the article.)

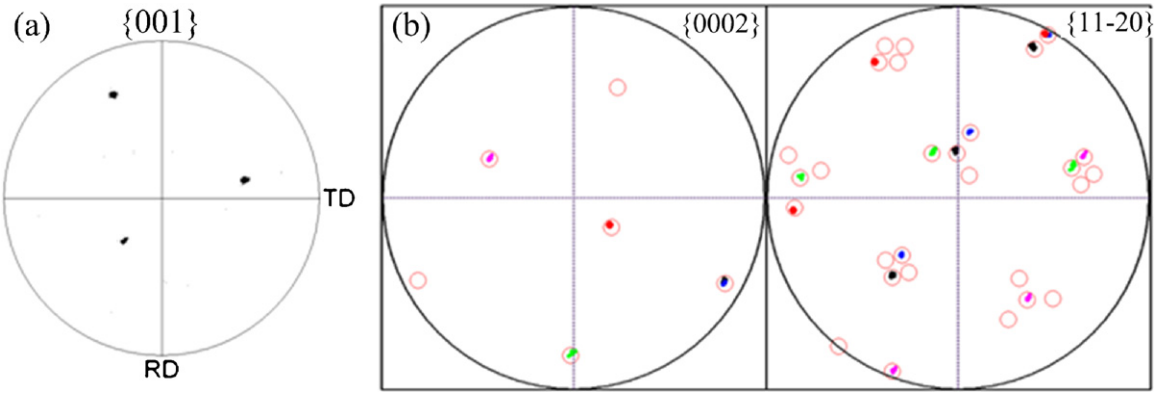

Fig. 8. (a) The {0 0 1} pole figure of residual β in marked "Grain D". (b) The {0 0 0 2} and {1 1 $\bar{2}$ 0} pole figures of α lamellae. The red circles and different color dots represent the theoretical calculation and experimental crystal orientation results of possible α variants in marked "Grain D". (For interpretation of the references to color in the figure caption and text, the reader is referred to the web version of the article.)

A and B, the Burgers OR is perfectly obeyed during β → α phase transformation in TA15 titanium alloy.

4. Discussion

According to our experimental results and analysis, the deformation strain, strain rate and subsequent cooling rate show a slight influence on the respecting of Burgers OR between the α lamellae/variants and matrix β phase during the α precipitation process. The possible reasons accounting for these results will be discussed in conjunction with grain-scale simulation results from crystal plasticity finite element method (CP-FEM) in this section.

4.1. Uniaxial compression deformation simulation

As mentioned in the introduction, many authors point out that the external factors, including prior deformation rate [12,13], strain field [13,14], stress [16], elastic anisotropy [15] and so on, have a significant influence on the morphology of transformed α, the β → α phase transformation kinetics and the respecting of Burgers OR between the primary α (α_p) and residual β phase (β_r) during α precipitation process in Titanium alloys. To evaluate the stress/strain special distribution at grain-scale during plastic deformation, the crystal plasticity finite element method (CP-FEM) was developed to simulate heterogeneous plastic deformation of polycrystalline titanium alloy in single β phase region. The Numerical formulation and verification of CP-FEM for fcc and bcc materials deformed by crystallographic slip can be found in references [19–22]. The constitutive model employed in the current study was developed by Peirce et al. [23] and by Asaro and Needleman [24]. The hyper secant hardening law was implemented to describe the self- and latent-hardening effects (see the full description [23] for details). This rate-dependent constitutive relationship was implemented into the user material subroutine UMAT in the commercial finite element code, ABAQUS/Standard [25].

The quasi 3-D model was created in ABAQUS/CAE, as shown in Fig. 9(a). Each grain was assigned an identical crystal orientation according to the retained β crystal orientation in test A (see Fig. 1(b)). For the simulation of uniaxial compression, prescribed displacement in the *Y* direction was imposed on the 1–4–8–5 face. The boundary conditions were applied to the three faces, as shown in Fig. 9(b). For β titanium with cubic crystal symmetry, three independent elastic constants (C_{11} = 97.7, C_{12} = 82.5, and C_{44} = 37.5 GPa) [26] were used in the present model. Actually, the elastic modulus

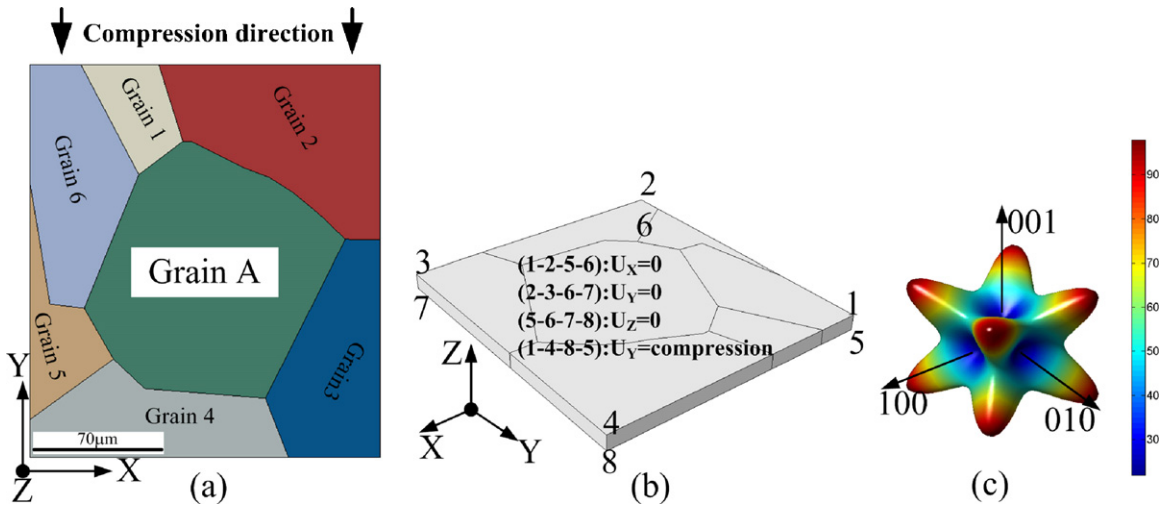

Fig. 9. (a) A mapping for the simulation of residual elastic strain concentration in deformed TA15 titanium alloy at 1050 °C. (b) Boundary condition for uniaxial compression. (c) Young's modulus surface plots of β Ti, the unit of the numbers on the color bar is GPa. (For interpretation of the references to color in the figure caption, the reader is referred to the web version of the article.)

Table 2
Microscopic hardening coefficients determined from the fitting procedure.

m	$\dot{\gamma}_0$	h_0	τ_0^α	τ_{sat}
0.1	0.001 s^{-1}	541.5 MPa	60.8 MPa	109.5 MPa

significantly varied along different crystallographic orientations, as shown the Young's modulus surface plots of β Ti in Fig. 9(c). Other parameters used in the CP-FEM simulation are listed in Table 2.

4.2. Spatial distributions of stress and strain at different deformation strains

Since the cropped region represents the small part of a larger body and boundary conditions considering neighboring grains are applied on surface (1–2–6–5), (2–3–7–6) and (1–4–8–5) which is related to grain (1–6), only the properties of "Grain A" are presented in our discussion. The spatial distributions of the elastic strain component-EE22 and stress component-S22 along compression direction at 0.1, 0.2, 0.3 deformation strains were shown in Fig. 10(a)–(f), respectively. Obviously, the strain distribution in "Grain A" and at grain boundaries is relatively homogeneous. With increasing compression deformation strain, although the mean values of EE22 is observed to increase steadily, the relative standard deviation, which is calculated by standard deviation deviating mean value, is relatively small (less than 20%) and almost constant. The error bars in EE22 and the evolutions of relative standard deviation are shown in Fig. 11.

Similarly, no significant stress concentration appeared in the "Grain A" interior or at its boundaries with the increase of the

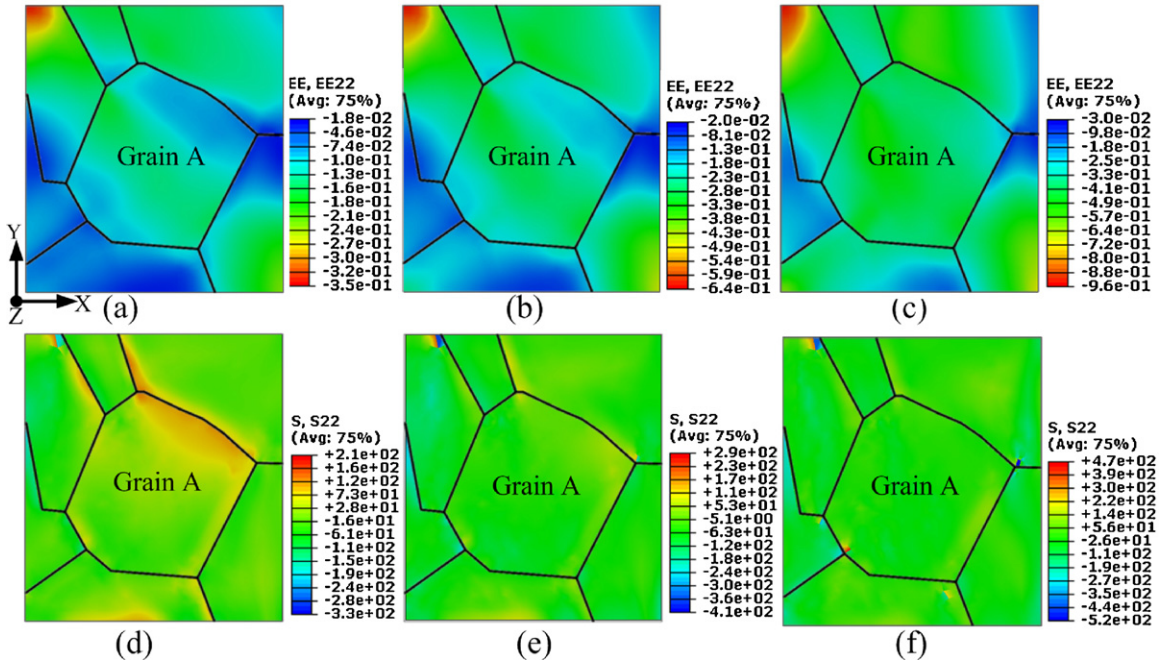

Fig. 10. Spatial distribution of the elastic strain component-EE22 and stress component-S22 after uniaxial compression at a compression strain of (a and d) 0.1, (b and e) 0.2 and (c and f) 0.3, at 1 s^{-1} strain rate, respectively.

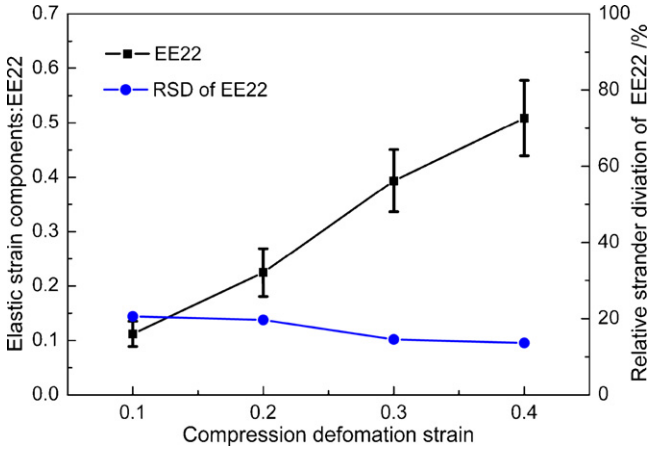

Fig. 11. The evolutions of elastic strain component-EE22 (along compression direction) and relative standard deviation (RSD) with increasing compression deformation strain at 1 s^{-1} strain rate.

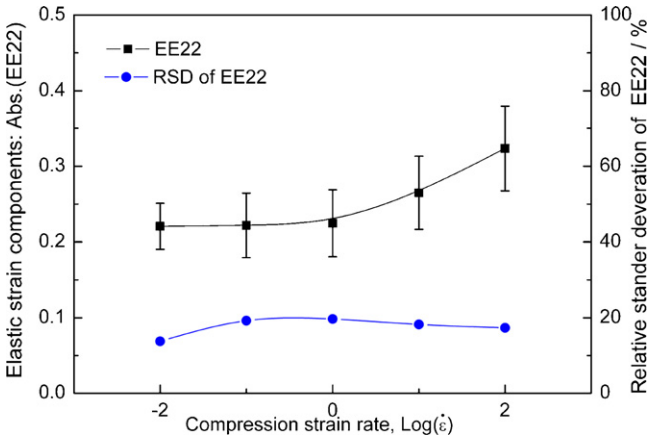

Fig. 13. The evolutions of strain component-EE22 (along compression direction) and relative standard deviation (RSD) of "Grain A" with increasing compression deformation strain rate, $\varepsilon = -0.2$.

deformation strain. It is worth noting that the spatial distribution of elastic stress component-EE22 shows relatively high positive value at the upper right "Grain A" boundary in the specimen deformed to a true strain of 0.1, as shown in Fig. 10(d). However, at the same time, the homogeneous stress gradient can be observed from the grain boundary to the grain interior. The statistical plotting of S22 in "Grain A" (as shown in Fig. 12) gives us a more clear illustration: each S22 distribution curve exhibits only one smooth single peak; although the peak values increase as the deformation strain increases, the values of peak width are very close for different deformation strains. These results indicate that the stress distribution in "Grain A" is relatively homogeneous and no heterogeneity is observed with increasing deformation strain.

4.3. Spatial distributions of stress and strain at different strain rates

The influences of strain rate on the strain component-EE22 and stress component-S22 are illustrated in Figs. 13 and 14, respectively. The mean values of EE22 are very close for the strain rate lower than 1 s^{-1}, but are significantly increased for strain rate between 1 s^{-1} and 100 s^{-1}. However, the relative standard deviations of EE22 still exhibit a small change with increasing strain rate, which means that the deformation strain rate has no obvious influence on the strain distribution homogeneity. Although the deformation strain rate increases from 0.01 to 100 s^{-1}, the peak widths of stress component-S22 distribution are relatively narrow, and are very close to each other, as shown in Fig. 14. These results indicate that the deformation rate has no obvious influence on stress distribution: no significant stress concentration appeared in the interior or at the boundary of the investigated "Grain A" during compression deformation process.

4.4. Influences of stress and strain anisotropy

Actually, according to other research results [15], it is not the elastic strain, but elastic anisotropy, which has a decisive influence on the variants selection during α precipitation from β phase. Here, according to our CP-FEM simulation results, no obvious elastic anisotropy or heterogeneity (including strain and stress components) has been detected in the interior or at the boundary of β "Grain A" which was subjected to different deformation strains. Similarly, deformation rate also shows very slight influence on stress/strain distribution: no significant concentration or anisotropy appeared in the investigated β "Grain A" as the strain rate was increased. This may be resulted from the relatively high symmetry of elastic property for bcc crystal and easy deformability of β phase (48 potential slip systems for bcc crystal and relative low critical resolved shear stress) at high temperature. The simulation results, which reveal the influences of deformation strain and strain rate on strain/stress anisotropy, to some extent explained the present experiment observation: the prior β deformation strain

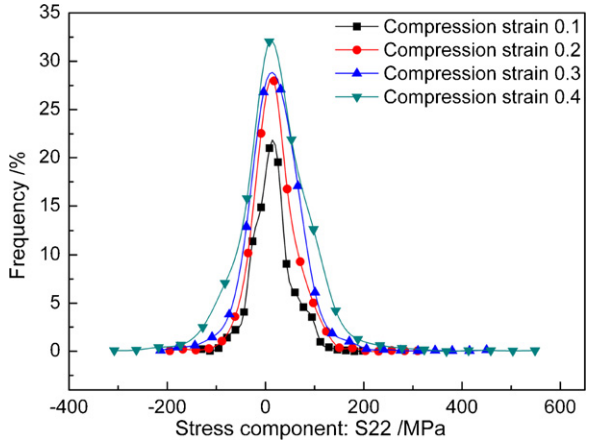

Fig. 12. The distributions of stress component-S22 (along compression direction) at different compression deformation strains, at 1 s^{-1} strain rate.

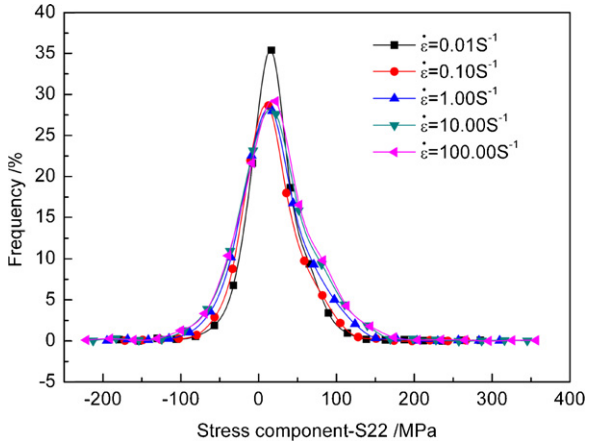

Fig. 14. The distribution of stress component-S22 (along compression direction) at different compression deformation strain rates, $\varepsilon = -0.2$.

and strain rate have no significant influence on the respecting of Burgers OR between the α lamellae/variants and matrix β phase during the α precipitation process.

Based on the experimental results and simulation analysis, we deduce that, the stress and strain heterogeneous or anisotropic distributions have a significant influence on the respecting of Burgers OR. The mean value of stress or strain, which affects the transformation kinetics [13,27–30], only have an obvious effect on microstructure morphology and size. Actually, this deduction was confirmed indirectly by other authors work. For example, when there exists sharp textures [14], such as macrozone, which usually lead to significant stress/strain localization, it was observed that just only 60% and 30% of the α_p/β boundaries obeyed the Burgers OR within macrozone and less textured macrozones, respectively [14]. On the other hand, our simulation results show that the mean values of EE22 are very close when the strain rate is lower than $1\,s^{-1}$ but are significantly increased for strain rate between $1\,s^{-1}$ and $100\,s^{-1}$. Obviously, this trend agrees well with experimental results which show that lamellar α grains are formed when the strain rate is less than $0.1\,s^{-1}$ and coarse equiaxed α grains are formed for strain rate between 1 and $100\,s^{-1}$ [12].

Regarding the cooling rate, there are two possible reasons accounting for the experimental observations. Firstly, the β phase has a relatively low modulus [31]. Secondly, the β deforming is usually performed at temperature of 30–50 °C above the β-transus [1]. Because of the low elastic modulus, a high symmetry for bcc system and a small range of temperature change, the cooling rate seems to have a very weak influence on stress/strain heterogeneity during the specimen cooling down from deformation temperature to β-transus. This is the main reason for maintenance of Burgers OR between the α precipitates and β phase during $\beta \rightarrow \alpha$ phase process under high cooling rate (50 °C/s). However, the cooling rate exhibits a significant influence on the $\beta \rightarrow \alpha$ phase transformation kinetics [11,32,33], including the nucleation sites, numbers and growth rates of the α precipitations, and this leads to the formation of fine α lamellae of sample C in the present study.

5. Conclusions

The compression deformations with different experimental parameters were conducted on TA15 titanium in single β phase region of the phase diagram. The microstructure morphologies and crystallographic orientations relationships were investigated by SEM/EBSD technique and analyzed by EDAX-TSL OIM® software. The influences of deformation strain, strain rate and subsequent cooling rate on the respecting of Burgers OR between the α lamellae/variants and matrix β phase during α precipitation process were studied. Their influences on the morphology of α lamellae were also compared. The influences of deformation strain and strain rate on stress/strain component distributions in interior of grain and at grain boundary were discussed using the CP-FEM grain-scale simulation results. Based on the experimental results and simulation analysis, the conclusions can be drawn as follows:

1. Without prior β deformation effect and at low cooling rate, the microstructure is composed of long α lamellae and residual β phase. Some of the α lamellae even cross the whole β grain. The Burgers OR is perfectly respected during the $\beta \rightarrow \alpha$ phase transformation.
2. With severe uniaxial compression deformation, no obvious β sub-grain was formed in the investigated "Grain B". There are no obvious changes in the morphology of α lamellae as compared with the undeformed situation. The deformation strain has no significant influence on the obeying of Burgers OR rule during $\beta \rightarrow \alpha$ phase transformation.
3. The cooling rate has a significant effect on the morphologies of α variants. The α lamellae become finer and shorter with increasing cooling rate. There are seldom α laths crossing the whole prior β grain when the cooling rate is as high as 50 °C/s. The orientations of α variants are slightly scattered and some of them even shift out of the ranges of calculated results. However, the Burgers OR rule is still generally respected during α precipitation process under high cooling rate situation.
4. The deformation strain rate has an obvious influence on the morphologies of α lamellae: the lengths of α lamellae decreases with increasing strain rate. At strain rate of $10\,s^{-1}$ in the present study, the lamellae crossing the whole prior β grain have not been found in marked "Grain D". However, similar to the deformation strain, the strain rate also has no significant influence on the obeying of Burgers OR rule.
5. The elastic strain/stress anisotropy but not the mean values of stress/strain has a significant influence on the respecting of Burgers OR. The mean values of stress/strain components are strongly increased as deformation strain is increased. The mean strain values (EE22) are very close when the strain rate is lower than $1\,s^{-1}$, while they are significantly increased for high strain rate between 1 and $100\,s^{-1}$. However, both the deformation strain and strain rate do not have an obvious influence on the elastic strain/stress anisotropy or heterogeneity in the grain interior and at the grain boundary of the investigated β "Grain A".

In general, the external factors, including prior β deformation strain, strain rate and cooling rate, have a slight influence on Burgers OR rule during $\beta \rightarrow \alpha$ phase transformation. However, factors of strain rate and cooling rate have a significant effect on the morphology of α phase.

Acknowledgements

The author (He Dong) gratefully acknowledges scholarship support from the China Scholarship Council (CSC). The author (He Dong) also wishes to thank Katja Angenendt and Monika Nellessen for their help with sample preparations and Dr. Li and Dr. B. Ravi Kumar for their language help.

References

[1] M.J. Donachie, Titanium: A Technical Guide, second ed., ASM International, Ohio, 1988.
[2] M. Peters, J. Hemptenmacher, J. Kumpfert, C. Leyens, in: C. Leyens, M. Peters (Eds.), Titanium and Titanium Alloys, Wiley-VCH Verlag GmbH & Co. KGaA, Weinheim, 2005, pp. 1–36.
[3] Z.C. Sun, H. Yang, G.J. Han, X.G. Fan, Mater. Sci. Eng. A: Struct. 527 (2010) 3464–3471.
[4] I. Weiss, S.L. Semiatin, Mater. Sci. Eng. A 263 (1999) 243–256.
[5] W.G. Burgers, Physica 1 (1934) 561–586.
[6] M.R. Daymond, R.A. Holt, S. Cai, P. Mosbrucker, S.C. Vogel, Acta Mater. 58 (2010) 4053–4066.
[7] I. Lonardelli, N. Gey, H.R. Wenk, M. Humbert, S.C. Vogel, L. Lutterotti, Acta Mater. 55 (2007) 5718–5727.
[8] C. Cayron, Scr. Mater. 59 (2008) 570–573.
[9] N. Stanford, P.S. Bate, Acta Mater. 52 (2004) 5215–5224.
[10] C. Leyens, M. Peters, Titanium and Titanium alloys, Wiley-VCH Verlag GmbH & Co., 2003, p. 532, ISBN: 3-527-30534-3.
[11] G. Lütjering, Mater. Sci. Eng. A 243 (1998) 32–45.
[12] T. Seshacharyulu, B. Dutta, Scr. Mater. 46 (2002) 673–678.
[13] J. Da Costa Teixeira, B. Appolaire, E. Aeby-Gautier, S. Denis, F. Bruneseaux, Acta Mater. 54 (2006) 4261–4271.
[14] L. Germain, N. Gey, M. Humbert, P. Vo, M. Jahazi, P. Bocher, Acta Mater. 56 (2008) 4298–4308.
[15] M. Humbert, L. Germain, N. Gey, P. Bocher, M. Jahazi, Mater. Sci. Eng. A 430 (2006) 157–164.
[16] M. Kato, S. Onaka, T. Fujii, Sci. Technol. Adv. Mater. 2 (2001) 375–380.
[17] M. Humbert, N. Gey, L. Germain, Mater. Sci. Forum 495–497 (2005) 1111–1120.
[18] D. Bhattacharyya, G.B. Viswanathan, R. Denkenberger, D. Furrer, H.L. Fraser, Acta Mater. 51 (2003) 4679–4691.
[19] D. Raabe, Z. Zhao, S.J. Park, F. Roters, Acta Mater. 50 (2002) 421–440.
[20] S.H. Choi, Acta Mater. 51 (2003) 1775–1788.

[21] R. Becker, S. Panchanadeeswaran, Acta Metall. Mater. 43 (1995) 2701–2719.
[22] G.B. Sarma, B. Radhakrishnan, T. Zacharia, Comp. Mater. Sci. 12 (1998) 105–123.
[23] D. Peirce, R.J. Asaro, A. Needleman, Acta Metall. Mater. 31 (1983) 1951–1976.
[24] R.J. Asaro, A. Needleman, Acta Metall. Mater. 33 (1985) 923–953.
[25] ABAQUS User's Manual, Version 6.5, Providence, Hibbit, Karlsson & Sorenson, RI, 2004.
[26] H. Ledbetter, J. Appl. Phys. 95 (2004) 4642.
[27] T. Eto, A. Sato, T. Mori, Acta Metall. Mater. 26 (1978) 499–508.
[28] Y. Tanaka, A. Sato, T. Mori, Acta Metall. Mater. 26 (1978) 529–540.
[29] Y. Higo, F. Lecroisey, T. Mori, Acta Metall. Mater. 22 (1974) 313–323.
[30] M. Kato, R. Monzen, T. Mori, Acta Metall. Mater. 26 (1978) 605–613.
[31] G. Lütjering, J.C. Williams, Titanium, Springer, Berlin, Heidelberg, 2007, pp. 259–282.
[32] T. Karthikeyan, A. Dasgupta, R. Khatirkar, S. Saroja, I. Samajdar, M. Vijayalakshmi, Mater. Sci. Eng. A 528 (2010) 549–558.
[33] S.K. Li, S.X. Hui, W.J. Ye, Y. Yu, B.Q. Xiong, Rare Met. Mater. Eng. 36 (2007) 786–789.